Pramāṇa, Vol. 9, No. 3, September 1977, pp. 283-296, © Printed in India.

ESR study of exchange coupled pairs in copper diethyldithiocarbamate—explanation of the low temperature hyperfine anomaly

C V MANJUNATH, KUMARI SANTOSH and R SRINIVASAN
Department of Physics, Indian Institute of Science, Bangalore 560 012

MS received 21 April 1977; revised 22 June 1977

Abstract. A study of the hyperfine interaction in the ESR of Cu-Cu pairs in single crystals of copper diethyldithiocarbamate as a function of temperature has shown distinct differences in the hyperfine structure in the two fine structure transitions at 20 K, the spectrum not having the same hyperfine intensity pattern in the low field fine structure transition in contrast to that of the high field transition. The details of the structure of both the fine structure transitions in the 20 K spectrum have now been explained by recognizing the fact that the mixing of the nuclear spin states caused by the anisotropic hyperfine interaction affects the electron spin states $|+1\rangle$ and $|-1\rangle$ differently. This has incidentally led to a determination of the sign of D confirming the earlier model. The anomalous hyperfine structure is found to become symmetric at 77 K and 300 K. It is proposed that the reason for this lies in the dynamics of spin-lattice interaction which limits the lifetime of the spin states in each of the electronic levels $|-1\rangle$, $|0\rangle$ and $|+1\rangle$. The estimate of spin-lattice relaxation time agrees with those indicated from other studies. The model proposed here for the hyperfine interaction of pairs in the electronic triplet state is of general validity.

Keywords. Electron spin resonance; exchange interaction; copper diethyldithiocarbamate; anisotropic hyperfine interaction; hyperfine intensity pattern; mixing of nuclear states; spin-lattice interaction.

1. Introduction

An X-band ESR study of exchange coupled pairs of copper ions in single crystals of copper diethyldithiocarbamate ($Cu(dtc)_2$) isomorphously diluted with the corresponding zinc salt, has been reported in the temperature range 4·2—300 K (Cowsik *et al* 1971; Cowsik and Srinivasan 1973). The exchange coupling was found to be ferromagnetic thus leaving a triplet ground state. The 300 K ESR spectrum consisted of an intense central group of lines due to isolated copper ions flanked on either side by weak lines from exchange coupled pairs of copper ions. Each fine structure transition in the exchange coupled spectrum was further split into seven hyperfine (h.f.) components in the intensity ratio 1 : 2 : 3 : 4 : 3 : 2 : 1 corresponding to equivalent coupling to the two copper nuclei ($I=3/2$) of the exchange coupled pair. The principal axes of the g and A tensors for the doublet and triplet spectra coincide. While the g values are approximately the same in all orientations, the h.f. separation for the coupled species is roughly half that for the isolated ion. This implies that

exchange is sufficiently fast to average the h.f. interaction to half that for the single ion.

ESR studies at low temperature were taken up mainly to determine J. Spectra were recorded with $H \| D_{max}$ (maximum zero field splitting in the ac plane) and $H \| D_z$ (the z-axis of the fine structure tensor), at various temperatures down to 4·2 K. A striking feature of the low temperature recording is the apparent inequivalence of the two fine structure transitions. Although the high field fine structure transition consists of hyperfine line intensities expected of two equivalently coupled copper nuclei, the low field transition is weaker and appears to be split into a large number of lines. In the next section we take up a discussion of the 20 K spectrum. In section 3 we discuss the spectrum at higher temperatures. We conclude by pointing out the applicability of some of the observations we have made here, to other situations.

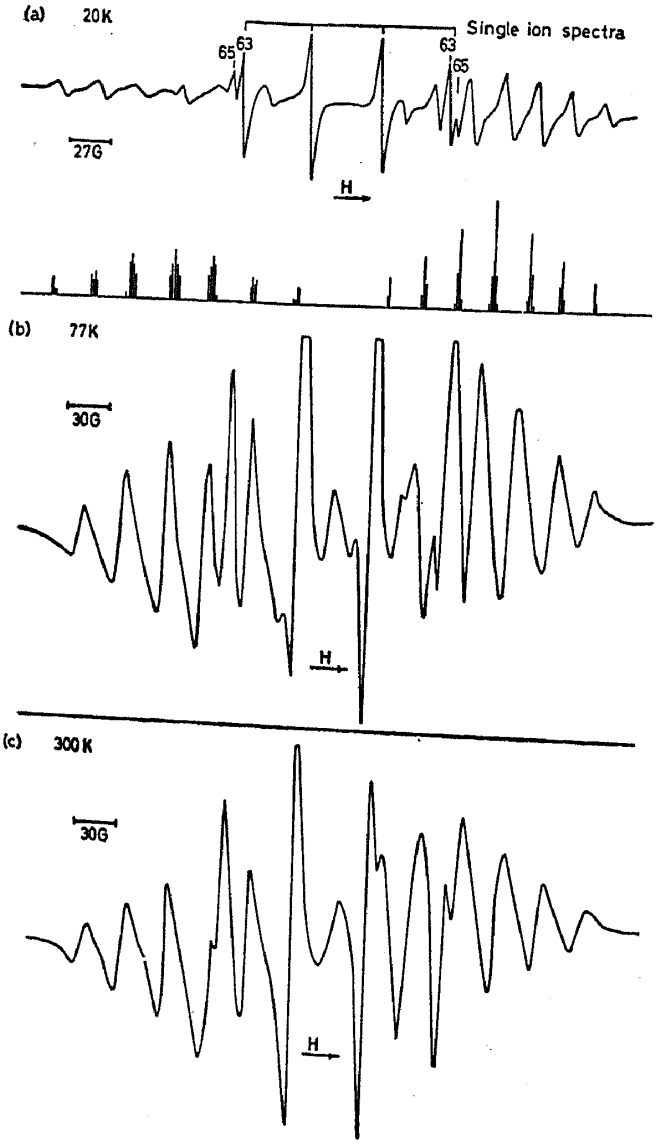

Figure 1. ESR spectra of copper diethyldithiocarbamate with $H \| D_{max}$ (a) at 20 K. The stick diagram shows the calculated spectrum (b) at 77 K and (c) at 300 K. Note the marked departure from 'equivalent coupling' in the low field component at 20 K.

2. 20 K spectrum

A recording of the 20 K spectrum for $H \| D_{max}$ is shown in figure 1a. The figure clearly shows the absence of hyperfine intensities in the ratio 1 : 2 : 3 : 4 : 3 : 2 : 1 in the low field fine structure transition quite unlike what is seen for the high field fine structure transition. Minakata and Iwasaki (1972) have examined a similar situation in free radical pairs where proton h.f. structure in the two fine structure components show differences.

For the electron spin multiplet system containing nuclear spins, the spin-Hamiltonian may be written as

$$\mathcal{H} = J\mathbf{S}_1 \cdot \mathbf{S}_2 + H\beta\,\mathbf{S} \cdot \boldsymbol{g} \cdot \mathbf{p} + \mathbf{S} \cdot \boldsymbol{D} \cdot \mathbf{S} + \sum_j N[\mathbf{S} \cdot \boldsymbol{A}_j \cdot \mathbf{I}_j] - \sum_j \nu_{nj}\, \mathbf{p} \cdot \mathbf{I}_j \tag{1}$$

where $\nu_{nj} = g_{nj}\beta_{nj} H/hc$ which, for copper nucleus at 9·3 GHz is $1{\cdot}29 \times 10^{-4}$ cm^{-1}. The successive terms on the right hand side represent the contributions from exchange, electronic Zeeman, electronic spin-spin, hyperfine and nuclear Zeeman interactions respectively. $\boldsymbol{D}$, J and $\boldsymbol{A}$ are given in wavenumber units, $\mathbf{p}$ is the unit vector along H, N is the constant parameter which relates the hyperfine coupling tensor in the doublet system (i.e., uncoupled ion) to that in the multiplet system (i.e., exchange coupled pair). In this case $N = 1/2$ as would be expected for a system with $J \gg A$ (Slichter 1955). It is shown in the appendix how the h.f. interaction leads to a situation where the electron spin is quantized along a direction different from that of the

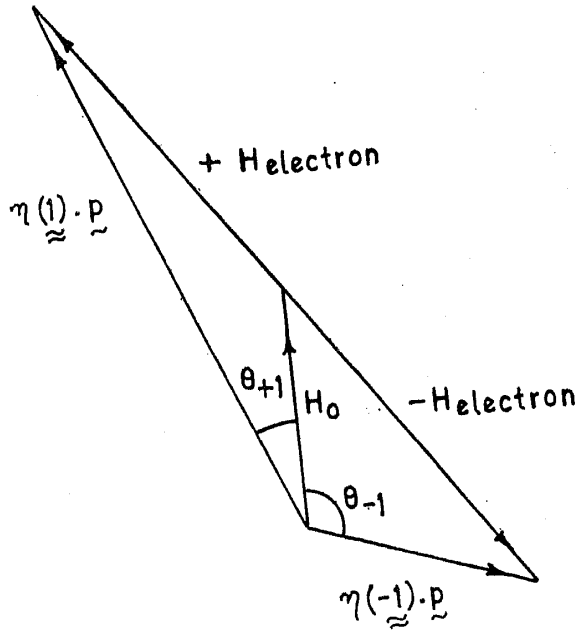

Figure 2. Diagram illustrating a case where the external magnetic field is applied away from the principal axes, the vector addition of the fields of the nucleus (1) due to the magnetic electrons ($H_{electron}$) and (2) due to the external magnetic field H_0. $\eta(+1)\,\mathbf{p}$ and $\eta(-1)\,\mathbf{p}$ are the directions of the resultant field along which the nuclei are quantized for the electronic levels $|+1\rangle$ and $|-1\rangle$ respectively. Note that the change in the orientation of the resultant field denoted by θ_{-1} and θ_{+1}, is more for the electronic transition $|0\rangle \longleftrightarrow |-1\rangle$ than for the transition $|0\rangle \longleftrightarrow |+1\rangle$.

Table 1. Relative intensities (I) and line positions for the lines shown in stick diagram in figure 1a

No.	Transition states	Electron transition $\|0\rangle \longleftrightarrow \|-1\rangle$		Electron transition $\|1\rangle \longleftrightarrow \|0\rangle$	
		Line position	I	Line position	I
1	(3/2, 3/2; 3/2, 3/2)	$\|\eta(-1)\|(3)-\|\eta(0)\|(3)$	3×10^{-5}	$\|\eta(0)\|(3)-\|\eta(1)\|(3)$	0·66
2	(3/2, 3/2; 3/2, 1/2), (3/2, 3/2; 1/2, 3/2)	$\|\eta(-1)\|(2)-\|\eta(0)\|(3)$	0·001	$\|\eta(0)\|(2)-\|\eta(1)\|(3)$	0·28
3	(3/2, 3/2; 3/2, −1/2), (3/2, 3/2; −1/2, 3/2), (3/2, 3/2; 1/2, 1/2)	$\|\eta(-1)\|(1)-\|\eta(0)\|(3)$	0·01	$\|\eta(0)\|(1)-\|\eta(1)\|(3)$	0·05
4	(3/2, 3/2; 3/2, −3/2), (3/2, 3/2; −3/2, 3/2), (3/2, 3/2; 1/2, −1/2) (3/2, 3/2; −1/2, 1/2)	$\|\eta(-1)\|(0)-\|\eta(0)\|(3)$	0·066	$\|\eta(0)\|(0)-\|\eta(1)\|(3)$	0·044
5	(3/2, 3/2; 1/2, −3/2), (3/2, 3/2; −3/2, 1/2), (3/2, 3/2; −1/2, −1/2)	$\|\eta(-1)\|(-1)-\|\eta(0)\|(3)$	0·21	$\|\eta(0)\|(-1)-\|\eta(1)\|(3)$	2×10^{-4}
6	(3/2, 3/2; −1/2, −3/2), (3/2, 3/2; −3/2, −1/2)	$\|\eta(-1)\|(-2)-\|\eta(0)\|(3)$	0·4	$\|\eta(0)\|(-2)-\|\eta(1)\|(3)$	8×10^{-6}
7	(3/2, 3/2; −3/2, −3/2)	$\|\eta(-1)\|(-3)-\|\eta(0)\|(3)$	0·31	$\|\eta(0)\|(-3)-\|\eta(1)\|(3)$	9×10^{-8}
8	(3/2, 1/2; 3/2, 3/2), (1/2, 3/2; 3/2, 3/2)	$\|\eta(-1)\|(3) \quad -\|\eta(0)\|(2)$	8×10^{-4}	$\|\eta(0)\|(3) \quad -\|\eta(1)\|(2)$	0·28
9	(3/2, 1/2; 3/2, 1/2), (1/2, 3/2; 3/2, 1/2), (3/2, 1/2; 1/2, 3/2), (1/2, 3/2; 1/2, 3/2)	$\|\eta(-1)\|(2)-\|\eta(0)\|(2)$	0·016	$\|\eta(0)\|(2)-\|\eta(1)\|(2)$	1·06
10	(3/2, 1/2; 3/2, −1/2), (1/2, 3/2; 3/2, −1/2), (3/2, 1/2; −1/2, 3/2) (1/2, 3/2; −1/2, 3/2), (3/2, 1/2; 1/2, 1/2), (1/2, 3/2; 1/2, 1/2)	$\|\eta(-1)\|(1)-\|\eta(0)\|(2)$	0·121	$\|\eta(0)\|(1)-\eta(1)\|(2)$	0·604
11	(3/2, 1/2; 3/2, −3/2), (1/2, 3/2; 3/2, −3/2), (3/2, 1/2; −3/2, 3/2), (1/2, 3/2; −3/2, 3/2), (3/2, 1/2; 1/2, −1/2), (1/2, 3/2; 1/2, −1/2) (3/2, 1/2; −1/2, 1/2), (1/2, 3/2; −1/2, 1/2)	$\|\eta(-1)\|(0)-\|\eta(0)\|(2)$	0·39	$\|\eta(0)\|(0)-\|\eta(1)\|(2)$	0·114
12	(3/2, 1/2; 1/2, −3/2), (1/2, 3/2; 1/2, −3/2), (3/2, 1/2; −3/2, 1/2), (1/2, 3/2; −3/2, 1/2), (1/2, 3/2; −1/2, −1/2), (3/2, 1/2; −1/2, −1/2)	$\|\eta(-1)\|(-1)-\|\eta(0)\|(2)$	1·066	$\|\eta(0)\|(-1)-\|\eta(1)\|(2)$	0·01
13	(3/2, 1/2; −1/2, −3/2), (1/2, 3/2; −1/2, −3/2), (3/2, 1/2; −3/2, −1/2), (1/2, 3/2; −3/2, −1/2)	$\|\eta(-1)\|(-2)-\|\eta(0)\|(2)$	0·42	$\|\eta(0)\|(-2)-\|\eta(1)\|(2)$	3×10^{-4}
14	(3/2, 1/2; −3/2, −3/2), (1/2, 3/2; −3/2, −3/2)	$\|\eta(-1)\|(-3)-\|\eta(0)\|(2)$	0·4	$\|\eta(0)\|(-3)-\|\eta(1)\|(2)$	6×10^{-6}
15	(3/2, −1/2; 3/2, 3/2), (−1/2, 3/2; 3/2, 3/2), (1/2, 1/2; 3/2, 3/2)	$\|\eta(-1)\|(3)-\|\eta(0)\|(1)$	0·01	$\|\eta(0)\|(3) \quad -\|\eta(1)\|(1)$	0·05
16	(3/2, −1/2; 3/2, 1/2), (−1/2, 3/2; 3/2, 1/2), (3/2, −1/2; 1/2, 3/2), (−1/2, 3/2; 1/2, 3/2), (1/2, 1/2; 3/2, 1/2), (1/2, 1/2; 1/2, 3/2)	$\|\eta(-1)\|(2)-\|\eta(0)\|(1)$	0·122	$\|\eta(0)\|(2)-\|\eta(1)\|(1)$	0·584
17	(3/2, −1/2; 3/2, −1/2), (−1/2, 3/2; 3/2, −1/2), (3/2, −1/2; −1/2, 3/2), (−1/2, 3/2; −1/2, 3/2), (3/2, −1/2; 1/2, 1/2), (−1/2, 3/2; 1/2, 1/2), (1/2, 1/2; 3/2, −1/2), (1/2, 1/2; −1/2, 3/2), (1/2, 1/2; 1/2, 1/2)	$\|\eta(-1)\|(1)-\|\eta(0)\|(1)$	0·463	$\|\eta(0)\|(1)-\|\eta(1)\|(1)$	1·51

Table 1—(*Contd.*)

18	(3/2, −1/2; 3/2, −3/2), (−1/2, 3/2; 3/2, −3/2), (3/2, −1/2; −3/2, 3/2), (−1/2, 3/2; −3/2, 3/2), (3/2, −1/2; 1/2, −1/2), (−1/2, 3/2; 1/2, −1/2), (3/2, −1/2; −1/2, 1/2), (−1/2, 3/2; −1/2, 1/2), (1/2, 1/2; 3/2, −3/2), (1/2, 1/2; −3/2, 3/2), (1/2, 1/2; 1/2, −1/2), (1/2, 1/2; −1/2, 1/2)	$\lvert\eta(-1)\rvert(0)-\lvert\eta(0)\rvert(1)$	0·757	$\lvert\eta(0)\rvert(0)-\lvert\eta(0)\rvert(1)$	0·77
19	(3/2, −1/2; 1/2, −3/2), (−1/2, 3/2; 1/2, −3/2), (3/2, −1/2; −3/2, 1/2), (−1/2, 3/2; −3/2, 1/2) (3/2, −1/2; −1/2, −1/2), (−1/2, 3/2; −1/2, −1/2), (1/2, 1/2; 1/2, −3/2), (1/2, 1/2; −3/2, 1/2), (1/2, 1/2; −1/2, −1/2)	$\lvert\eta(-1)\rvert(-1)-\lvert\eta(0)\rvert(1)$	0·522	$\lvert\eta(0)\rvert(-1)-\lvert\eta(1)\rvert(1)$	0·138
20	(1/2, 1/2; −1/2, −3/2), (1/2, 1/2; −3/2, −1/2), (3/2, −1/2; −1/2, −3/2), (−1/2, 3/2; −1/2, −3/2), (3/2, −1/2; −3/2, −1/2), (−1/2, 3/2; −3/2, −1/2)	$\lvert\eta(-1)\rvert(-2)-\lvert\eta(0)\rvert(1)$	0·58	$\lvert\eta(0)\rvert(-2)-\lvert\eta(1)\rvert(1)$	0·004
21	(3/2, −1/2; −3/2, −3/2), (−1/2, 3/2; −3/2, −3/2), (1/2, 1/2; −3/2, −3/2)	$\lvert\eta(-1)\rvert(-3)-\lvert\eta(0)\rvert(1)$	0·17	$\lvert\eta(0)\rvert(-3)-\lvert\eta(1)\rvert(1)$	0·006
22	(3/2, −3/2; 3/2, 3/2), (−3/2, 3/2; 3/2, 3/2), (1/2, −1/2; 3/2, 3/2), (−1/2, 1/2; 3/2, 3/2)	$\lvert\eta(-1)\rvert(3)-\lvert\eta(0)\rvert(0)$	0·145	$\lvert\eta(0)\rvert(3)-\lvert\eta(1)\rvert(0)$	0·004
23	(3/2, −3/2; 3/2, 1/2), (−3/2, 3/2; 3/2, 1/2), (3/2, −3/2; 1/2, 3/2), (−3/2, 3/2; 1/2, 3/2), (1/2, −1/2; 3/2, 1/2), (−1/2, 1/2; 3/2, 1/2), (1/2, −1/2; 1/2, 3/2), (−1/2, 1/2; 1/2, 3/2)	$\lvert\eta(-1)\rvert(2)-\lvert\eta(0)\rvert(0)$	0·308	$\lvert\eta(0)\rvert(2)-\lvert\eta(1)\rvert(0)$	0·094
24	(3/2, −3/2; 3/2, −1/2), (−3/2, 3/2; 3/2, −1/2), (−3/2, 3/2; −1/2, 3/2), (3/2, −3/2; −1/2, 3/2), (3/2, −3/2; 1/2, 1/2), (−3/2, 3/2; 1/2, 1/2), (1/2, −1/2; 3/2, −1/2), (−1/2, 1/2; 3/2, −1/2), (1/2, −1/2; −1/2, 3/2), (−1/2, 1/2; −1/2, 3/2), (1/2, −1/2; 1/2, 1/2), (−1/2, 1/2; 1/2, 1/2)	$\lvert\eta(-1)\rvert(1)-\lvert\eta(0)\rvert(0)$	0·781	$\lvert\eta(0)\rvert(1)-\lvert\eta(1)\rvert(0)$	0·77
25	(3/2, −3/2; 3/2, −3/2), (−3/2, 3/2; 3/2, −3/2), (3/2, −3/2; −3/2, 3/2), (−3/2, 3/2; −3/2, 3/2), (3/2, −3/2; 1/2, −1/2), (−3/2, 3/2; 1/2, −1/2), (3/2, −3/2; −1/2, 1/2), (−3/2, 3/2; −1/2, 1/2), (1/2, −1/2; 3/2, −3/2), (−1/2, 1/2; 3/2, −3/2), (1/2, −1/2; −3/2, 3/2), (−1/2, 1/2; −3/2, 3/2) (1/2, −1/2; 1/2, −1/2), (−1/2, 1/2; 1/2, −1/2), (1/2, −1/2; −1/2, 1/2), (−1/2, 1/2; −1/2, 1/2)	$\lvert\eta(-1)\rvert(0)-\lvert\eta(0)\rvert(0)$	1·37	$\lvert\eta(0)\rvert(0)-\lvert\eta(1)\rvert(0)$	2·24

Table 1—(*Contd.*)

No	Transition states	Electron transition $\|0\rangle \longleftrightarrow \|-1\rangle$		Electron transition $\|1\rangle \longleftrightarrow \|0\rangle$	
		Line position	I	Line position	I
26	(3/2, −3/2; 1/2, −3/2), (−3/2, 3/2; 1/2, −3/2), (3/2, −3/2; −3/2, 1/2), (−3/2, 3/2; −3/2, 1/2), (3/2, −3/2; −1/2, −1/2), (−3/2, 3/2; −1/2, −1/2), (1/2, −1/2; 1/2, −3/2), (−1/2, 1/2; 1/2, −3/2), (1/2, −1/2; −3/2, 1/2), (−1/2, 1/2; −3/2, 1/2), (1/2, −1/2; −1/2, −1/2), (−1/2, 1/2; −1/2, −1/2)	$\|\eta(1)\|(-1)-\|\eta(0)\|(0)$	0·721	$\|\eta(0)\|(-1)-\|\eta(1)\|(0)$	0·770
27	(3/2, −3/2; −1/2, −3/2), (−3/2, 3/2; −1/2, −3/2), (3/2, −3/2; −3/2, −1/2), (−3/2, 3/2; −3/2, −1/2), (1/2, −1/2; −1/2, −3/2), (−1/2, 1/2; −1/2, −3/2), (1/2, −1/2; −3/2, −1/2), (−1/2, 1/2; −3/2, −1/2)	$\|\eta(1)\|(-2)-\|\eta(0)\|(0)$	0·30	$\|\eta(0)\|(-2)-\|\eta(1)\|(0)$	0·114
28	(3/2, −3/2; −3/2, −3/2), (−3/2, 3/2; −3/2, −3/2), (1/2, −1/2; −3/2, −3/2), (−1/2, 1/2; −3/2, −3/2)	$\|\eta(-1)\|(-3)-\|\eta(0)\|(0)$	0·144	$\|\eta(0)\|(-3)-\|\eta(1)\|(0)$	0·004
29	(1/2, −3/2; 3/2, 3/2), (−3/2, 1/2; 3/2, 3/2), (−1/2, −1/2; 3/2, 3/2)	$\|\eta(-1)\|(3)-\|\eta(0)\|(-1)$	0·21	$\|\eta(0)\|(3)-\|\eta(1)\|(-1)$	2×10^{-4}
30	(1/2, −3/2; 3/2, 1/2), (−3/2, 1/2; 3/2, 1/2), (1/2, −3/2; 1/2, 3/2), (−3/2, 1/2; 1/2, 3/2), (−1/2, −1/2; 3/2, 1/2), (−1/2, −1/2; 1/2, 3/2)	$\|\eta(-1)\|(2)-\|\eta(0)\|(-1)$	0·58	$\|\eta(0)\|(2)-\|\eta(1)\|(-1)$	0·01
31	(1/2, −3/2; 3/2, −1/2), (−3/2, 1/2; 3/2, −1/2), (1/2, −3/2; −1/2, 3/2), (−3/2, 1/2; −1/2, 3/2), (1/2, −3/2; 1/2, 1/2), (−3/2, 1/2; 1/2, 1/2) (−1/2, −1/2; 3/2, −1/2), (−1/2, −1/2; −1/2, 3/2), (−1/2, −1/2; 1/2, 1/2)	$\|\eta(-1)\|(1)-\|\eta(0)\|(-1)$	0·562	$\|\eta(0)\|(1)-\|\eta(1)\|(-1)$	0·142
32	(1/2, −3/2; 3/2, −3/2), (−3/2, 1/2; 3/2, −3/2), (1/2, −3/2; −3/2, 3/2), (−3/2, 1/2; −3/2, 3/2), (1/2, −3/2; 1/2, −1/2), (−3/2, 1/2; 1/2, −1/2), (1/2, −3/2; 1/2, 1/2), (−3/2, 1/2; −1/2, 1/2), (−1/2, −1/2; 3/2, −3/2), (−1/2, −1/2; −3/2, 3/2), (−1/2, −1/2; 1/2, −1/2), (−1/2, −1/2; −1/2, 1/2)	$\|\eta(-1)\|(0)-\|\eta(0)\|(-1)$	0·767	$\|\eta(0)\|(0)-\|\eta(1)\|(-1)$	0·77
33	(1/2, −3/2; 1/2, −3/2), (−3/2, 1/2; 1/2, −3/2), (1/2, −3/2; 3/2, 1/2)+, (−3/2, 1/2; −3/2, 1/2)+, (1/2, −3/2; −1/2, −1/2), (−3/2, 1/2; −1/2, −1/2) (1/2, −1/2; 1/2, −3/2), (−1/2, −1/2; −3/2,1/2), (1/2, −1/2; 1/2, −1/2);	$\|\eta(-1)\|(-1)-\|\eta(0)\|(-1)$	0·463	$\|\eta(0)\|(-1)-\|\eta(1)\|(-1)$	1·69

Table 1—(*Contd.*)

34	(−1/2, −1/2; −1/2, −3/2), (−1/2, −1/2; −3/2, −1/2), (1/2, −3/2; −1/2, −3/2), (−3/2, 1/2; −1/2, −3/2), (1/2, −3/2; −3/2, −1/2), (−3/2, 1/2; −3/2, −1/2)	$\|\eta(-1)\|(-2)-\|\eta(0)\|(-1)$	0·126	$\|\eta(0)\|(-2)-\|\eta(1)\|(-1)$	0·2
35	(1/2, −3/2; −3/2, −3/2), (−3/2, 1/2; −3/2, −3/2), (−1/2, −1/2; −3/2, −3/2)	$\|\eta(-1)\|(-3)-\|\eta(0)\|(-1)$	0·008	$\|\eta(0)\|(-3)-\|\eta(1)\|(-1)$	0·05
36	(−1/2, −3/2; 3/2, 3/2), (−3/2, −1/2; 3/2, 3/2)	$\|\eta(-1)\|(3)-\|\eta(0)\|(-2)$	0·4	$\|\eta(0)\|(3)-\|\eta(1)\|(-2)$	8×10^{-6}
37	(−1/2, −3/2; 3/2, 1/2), (−3/2, −1/2; 3/2, 1/2), (−1/2, −3/2; 1/2, 3/2), (−3/2, −1/2; 1/2, 3/2)	$\|\eta(-1)\|(2)-\|\eta(0)\|(-2)$	0·46	$\|\eta(0)\|(2)-\|\eta(1)\|(-2)$	4×10^{-4}
38	(−1/2, −3/2; 1/2, 1/2), (−3/2, −1/2; 1/2, 1/2), (−1/2, −3/2; 3/2, −1/2), (−3/2, −1/2; 3/2, −1/2), (−1/2, −3/2; −1/2, 3/2), (−3/2, −1/2; −1/2, 3/2)	$\|\eta(-1)\|(1)-\|\eta(0)\|(-2)$	1·026	$\|\eta(0)\|(1)-\|\eta(1)\|(-2)$	0·01
39	(−1/2, −3/2; 3/2, −3/2), (−3/2, −1/2; 3/2, −3/2), (−1/2, −3/2; −3/2, 3/2), (−3/2, −1/2; −3/2, 3/2), (−1/2, −3/2; 1/2, −1/2), (−3/2, −1/2; 1/2, −1/2), (−1/2, −3/2; −1/2, 1/2), (−3/2, −1/2; −1/2, 1/2)	$\|\eta(-1)\|(0)-\|\eta(0)\|(-2)$	0·384	$\|\eta(0)\|(0)-\|\eta(1)\|(-2)$	0·120
40	(−1/2, −3/2; 1/2, −3/2), (−3/2, −1/2; 1/2, −3/2), (−1/2, −3/2; −3/2, 1/2), (−3/2, −1/2; −3/2, 1/2), (−1/2, −3/2; −1/2, −1/2), (−3/2, −1/2; −1/2, 1/2)	$\|\eta(-1)\|(-1)-\|\eta(0)\|(-2)$	0·122	$\|\eta(0)\|(-1)-\|\eta(1)\|(-2)$	0·584
41	(−1/2, −3/2; −1/2, −3/2), (−3/2, −1/2; −1/2, −3/2), (−1/2, −3/2; −3/2, −1/2), (−3/2, −1/2; −3/2, −1/2)	$\|\eta(-1)\|(-2)-\|\eta(0)\|(-2)$	0·016	$\|\eta(0)\|(-2)-\|\eta(1)\|(-2)$	1·06
42	(−1/2, −3/2; −3/2, −3/2), (−3/2, −1/2; −3/2, −3/2)	$\|\eta(-1)\|(-3)-\|\eta(0)\|(-2)$	8×10^{-4}	$\|\eta(0)\|(-3)-\|\eta(1)\|(-2)$	0·28
43	(−3/2, −3/2; 3/2, 3/2)	$\|\eta(-1)\|(3)-\|\eta(0)\|(-3)$	0·3	$\|\eta(0)\|(3)-\|\eta(1)\|(-3)$	9×10^{-8}
44	(−3/2, −3/2; 3/2, 1/2), (−3/2, −3/2; 1/2, 3/2)	$\|\eta(-1)\|(2)-\|\eta(0)\|(-3)$	0·4	$\|\eta(0)\|(2)-\|\eta(1)\|(-3)$	8×10^{-6}
45	(−3/2, −3/2; 3/2, −1/2), (−3/2, −3/2; −1/2, 3/2), (−3/2, −3/2; 1/2, 1/2)	$\|\eta(-1)\|(1)-\|\eta(0)\|(-3)$	0·21	$\|\eta(0)\|(1)-\|\eta(1)\|(-3)$	2×10^{-4}
46	(−3/2, −3/2; 3/2, −3/2), (−3/2, −3/2; −3/2, 3/2), (−3/2, −3/2; 1/2, −1/2), (−3/2, −3/2; 1/2, 1/2)	$\|\eta(-1)\|(0)-\|\eta(0)\|(-3)$	0·066	$\|\eta(0)\|(0)-\|\eta(1)\|(-3)$	0·044
47	(−3/2, −3/2; −1/2, −1/2), (−3/2, −3/2; 1/2, −3/2), (−3/2, −3/2; −3/2, 1/2)	$\|\eta(-1)\|(-1)-\|\eta(0)\|(-3)$	0·01	$\|\eta(0)\|(-1)-\|\eta(1)\|(-3)$	0·05
48	(−3/2, −3/2; −1/2, −3/2), (−3/2, −3/2; −3/2, −1/2)	$\|\eta(-1)\|(-2)-\|\eta(0)\|(-3)$	0·001	$\|\eta(0)\|(-2)-\|\eta(1)\|(-3)$	0·28
49	(−3/2, −3/2; −3/2, −3/2)	$\|\eta(-1)\|(-3)-\|\eta(0)\|(-3)$	3×10^{-5}	$\|\eta(0)\|(-3)-\|\eta(1)\|(-3)$	0·66

applied field H. In fact, it turns out that the orientations of the electron spin in the $M = |+1\rangle$ and $|-1\rangle$ differ by an angle which is in general different from 180° (see figure 2). This means that in the allowed transition $|0\rangle \leftrightarrow |1\rangle$ and $|0\rangle \leftrightarrow |-1\rangle$, the direction of the electron quantization changes. This has the effect of mixing nuclear spin states as explained in the appendix and causes forbidden transitions. The intensities of all the forbidden as well as allowed transitions is calculated for a particular case as shown in the appendix and listed in the table 1.

The total number of possible combination of $(m_1(M)m_2(M); m'_1(M-1)\ m'_2(M-1))$ for a case where $I = 3/2$ is 256 and are given in table 1. The positions of the hyperfine lines with respect to the centre of each fine structure transition and the intensities of the hyperfine lines for $H \parallel D_{max}$ are also given in table 1.

Figure 1a shows the 20 K ESR spectrum for $H \parallel D_{max}$. The intense lines at the centre are due to the isolated copper ion. The outer lines are due to the Cu-Cu pair. The differences in the intensities of the hyperfine lines in the two fine structure transitions are clearly seen. The stick diagram drawn in accordance with the above calculations is shown below the spectrum. The absence of strong allowed lines in the low field pattern is clearly seen.

It has thus been shown that the $|0\rangle \leftrightarrow |-1\rangle$ transition is the one which contains forbidden lines. The spectrum shows that the forbidden h.f. lines appear in the low field fine structure transition which must therefore be the $|0\rangle \leftrightarrow |-1\rangle$ transition. The unambiguous fixing of the low field fine structure transition as the $|0\rangle \leftrightarrow |-1\rangle$ transition clearly shows that the sign of D must be negative as was inferred by the earlier authors (Cowsik and Srinivasan 1973).

3. 77 K and 300 K spectra

Figure 1b shows a recording of the spectrum at 77 K for $H \parallel D_{max}$ in the ac plane.

The h.f. tensor continues to be anisotropic at this temperature also, as noted by the earlier authors (Cowsik and Srinivasan 1973). It is therefore natural to expect forbidden lines at this temperature also as the forbidden lines appear due to the mixing of nuclear spin states by the anisotropic hyperfine interaction. But figure 1b clearly shows that the anomalies caused by the forbidden transitions do not exist and the spectrum has the intensity distribution expected from equivalent coupling to two copper nuclei. It was concluded that the explanation for the disappearance of the forbidden lines at 77 K must be found in the dynamics of the orientations of the nuclear quantization vector resulting in the different orientations of which being averaged out. Such a situation will give rise to nuclear spin states which are pure in all the electronic levels thus ruling out the possibility of observation of forbidden transitions.

The field experienced by the nucleus is the sum of the externally applied d.c. field and the field produced by the surrounding magnetic electrons. The nuclear spin is quantized along the axis defined by the resultant of the above fields. As was already seen in the preceding section, the nuclear quantization vector is oriented differently depending on the state of the electron. The rate at which this direction changes is determined by the lifetime of the spin state which in turn is determined by the spin lattice relaxation time (T_1). At very low temperatures around 20 K, T_1 is very long.

Let us suppose that T_1 is longer than 10^{-6} sec which is the inverse of the Zeeman frequency of the copper nuclei. The time 10^{-6} sec determines the upper limit to the rate of any interaction to which the copper nucleus can respond. Thus, at these temperatures the nuclear quantum states are quantized along different directions resulting in a mixing of the nuclear states and hence giving rise to forbidden transitions. As the temperature is raised from 20 K, the spin-lattice interaction increases mainly by the Raman process and hence, T_1 decreases and may become smaller than 10^{-6} sec. The nuclear quantization vector is changing directions at a rate which is too fast for the nucleus to respond to and hence the effect is averaged out. This would lead to the nuclear spin quantum number being once more a good quantum number in all the electronic transitions. Figure 1c which is a spectrum at 300 K also shows the same features of equivalent coupling to two copper nuclei with no forbidden hyperfine transitions.

It must be emphasized that the changes in lineshape observed on increasing the temperature from 20 K cannot be understood merely in terms of a broadening of all lines which is expected as a general result of shortened spin-lattice relaxation time. The specific effects of spin lattice relaxation pointed out here lead to a disappearance of forbidden transitions with the consequent growth in intensity of the allowed lines.

The disappearance of forbidden transitions at 77 K and 300 K forms a very interesting method, for the estimation of spin-lattice relaxation time. Since the anomalous h.f. spectrum exists at 20 K, it is implied from the foregoing argument that T_1 has to be longer than the inverse of the nuclear Zeeman frequency, which, for copper, is of the order of 10^{-6} sec. Al'tshuler *et al* (1975) have studied the spin-lattice relaxation of single ions and pairs in $Cu(dtc)_2$ in the temperature range 4·2—50 K. Their measurements agree very well with the model proposed here. T_1 at 20 K for pairs is 10^{-4} sec. This is longer than the inverse of the Zeeman frequency of copper nuclei (which is of the order of 10^{-6} sec) and hence, the different hyperfine field directions of the different electronic states is felt by the copper nuclei. Although Al'tshuler *et al* (1975) have not followed T_1 of pairs to higher temperatures (and shorter relaxation times), it is possible to see by extrapolation of their measurements that T_1 for pairs would be shorter than 10^{-6} sec at 77 K, thus fulfilling the condition necessary for the averaging proposed here.

4. Application to other systems

The model proposed here for the h.f. interaction of pairs in the electronic triplet state is clearly of general validity. Free radicals have very little orbital contribution to the ground state and hence have long T_1 in the range 10^{-4} to 10^{-5} sec at 77 K. The h.f. structure involved is that of protons, whose Zeeman frequency is larger than that of copper considered here. Therefore, one has to go to higher temperatures before the spin-lattice relaxation time becomes shorter than the inverse of the proton Zeeman frequency. Hence, it is possible to see anomalous h.f.s. in free radical pair spectra even at 77 K. However, it is unlikely that it will be observable at room temperature in any of these systems. Transition metal systems which involve larger orbital contributions than free radicals (hence shorter T_1) are rarely likely to show the anomaly even at 77 K. In fact, in $Ag(dtc)_2$ pairs (Van Rens *et al* 1972), T_1 is much shorter than in $Cu(dtc)_2$ and the pair spectrum is not seen at all above 130 K.

Studies using higher microwave frequency will naturally involve higher magnetic field and this will make the nuclear Zeeman interaction term larger. Thus it is noticed that in the case of proton structure in free radicals, increase of the microwave frequency from *X*-band to *Q*-band is sufficient to allow the nuclear Zeeman term to predominate over the hyperfine field term, thus removing the anomalous hyperfine structure. Thus, the increased Zeeman frequency (at any given temperature) will make the observation of the ' averaged h.f.s.' more probable. This is precisely what is observed for free radical pairs where the nuclei involved are protons (higher gyromagnetic ratio). There are, however, other cases involving nuclei with low gyromagnetic ratio, but involved in strong h.f. coupling as in the present case where increasing the EPR frequency does not remove the anomaly completely. (see for example, the *Q*-band spectrum of $Cu(dtc)_2$ pairs (Al'tshuler *et al* 1975), where the low field fine structure component is distinctly poorly resolved compared to the high field component).

5. Conclusions

In this paper we have shown how in triplet species it is possible to see anomalous hyperfine structure in the fine structure components and how such a study helps in the determination of the sign of the zero field splitting tensor. Further, we have pointed out here, for the first time, why in some circumstances this anomaly is not seen, and how this leads to certain inferences regarding spin lattice interaction of the pair.

Appendix

Only the last two terms of the Hamiltonian(1) will be considered as the perturbing Hamiltonian, as we are interested in the forbidden as well as allowed transitions arising from the mixing of the nuclear spin states by the anisotropic h.f. interaction.

The perturbing Hamiltonian is

$$\mathcal{H}' = \sum_j -\nu_{nj}\,\mathbf{p}\cdot\mathbf{I}_j + \sum_j \mathbf{S}\cdot(N\mathbf{A}_j)\cdot\mathbf{I}_j. \tag{A.1}$$

For the case where the magnetic field is applied in the plane which contains the z and x axes of the spin-Hamiltonian, the direction cosines of $\mathbf{p}$ are (sin θ, 0, cos θ) where θ is the angle between the z axis and the magnetic field direction.

The electron spin is quantized along the vector $\boldsymbol{g}\cdot\mathbf{p}$, the unit vector $\mathbf{u}$ along which is given by,

$$\mathbf{u} = \boldsymbol{g}.\mathbf{p}/|g| \tag{A.2}$$

where

$$|g| = \sqrt{\mathbf{p}.\boldsymbol{g}^2.\mathbf{p}} = (g_\parallel^2\cos^2\theta + g_\perp^2\sin^2\theta)^{1/2}. \tag{A.3}$$

For the $Cu(dtc)_2$ system, the values of g and A tensors of the pair at 20 K are $g_\parallel = 2{\cdot}062$, $g_\perp = 2{\cdot}056$, $A_\parallel = -124\times10^{-4}$ cm^{-1} and $A_\perp = -24\times10^{-4}$ cm^{-1}.

Hence,

$$\mathbf{u} = \begin{pmatrix} 2{\cdot}056 \sin\theta \\ 0 \\ 2{\cdot}062 \cos\theta \end{pmatrix} \Big/ |g| \,.$$

Assuming that the components of S perpendicular to **u** can be neglected, it is a good approximation to write the following first order perturbing Hamiltonian

$$\begin{aligned} \mathcal{H}' &= -\Sigma_j \left[\nu_{nj}\,\mathbf{p} - \mathbf{u}\,S\cdot(N\boldsymbol{A}_j)\right]\cdot\mathbf{I}_j \\ &= -\sum_j \eta_j\,(S)\cdot\mathbf{p}\cdot\mathbf{I}_j \end{aligned} \tag{A.4}$$

where $S = \mathbf{S}\cdot\mathbf{u}$ and $\eta_j\,(S) = \nu_{nj}\,\boldsymbol{E} - |g|^{-1}\,SN(\boldsymbol{g}.\boldsymbol{A}_j)$ and $\boldsymbol{E}$ is the unit tensor. Substituting the values of $\boldsymbol{g}$, $\boldsymbol{A}_j$ and ν_{nj}, we get,

$$\eta_j\,(S) = 10^{-4}\begin{pmatrix} 1{\cdot}29 + \dfrac{24{\cdot}6\,S}{|g|} & 0 & 0 \\ 0 & 1{\cdot}29 + \dfrac{24{\cdot}6\,S}{|g|} & 0 \\ 0 & 0 & 1{\cdot}29 + \dfrac{127{\cdot}8\,S}{|g|} \end{pmatrix}. \tag{A.5}$$

Since $\eta_j\,(S)\cdot\mathbf{p}$ is the sum of the hyperfine and external fields at the j-th nucleus, the nuclear spin $\mathbf{I}_j$ is quantized along the vector $\eta_j(S)\cdot\mathbf{p}$, the unit vector ξ_j of which is given by

$$\xi_j(S) \quad = \eta_j(S).\mathbf{p}/\,|\,\eta_j\,(S)\,| \tag{A.6}$$

where,

$$\begin{aligned} |\,\eta_j(S)| \;&= (\mathbf{p}.\,\eta_j{}^2\,(S).\mathbf{p})^{1/2} \\ &= 10^{-4}\left(\sin^2\theta\left(1{\cdot}29 + \frac{24{\cdot}6\,S}{|g|}\right)^2 + \cos^2\theta\left(1{\cdot}29 + \frac{127{\cdot}8\,S}{|g|}\right)^2\right)^{1/2}. \end{aligned} \tag{A.7}$$

Then the perturbing spin-Hamiltonian becomes,

$$\mathcal{H}' = -\sum_j |\,\eta_j(S)|\, I\xi_j(S) \tag{A.8}$$

where,

$$I\xi_j\,(S) = \mathbf{I}_j\cdot\xi_j\,(S).$$

If $|\,M\rangle$ is the eigenfunction of S with the eigenvalue M, and $|\,m_j\,(M)\rangle$ is the eigenfunction of $I\xi_j\,(M)$ with the eigenvalue $m_j\,(M)$, the first order energy is,

$$\begin{aligned} E'[M, m_1(M), m_2(M)] &= \langle M, m_1(M), m_2(M)|\,\mathcal{H}'\,|\,M, m_1(M), m_2(M)\rangle \\ &= -\Sigma\,|\,\eta_j(M)|\,m_j(M) \end{aligned}$$

$$= -\Sigma\left[10^{-4}\left(\sin^2\theta\left(1.29+\frac{24{\cdot}7\,M}{|g|}\right)^2\right.\right.$$

$$\left.\left.+\cos^2\theta\left(1{\cdot}29+\frac{127{\cdot}8\,M}{|g|}\right)^2\right)^{1/2} m_j(M)\right]. \qquad \text{(A.9)}$$

The important point to be noted here is that the usual selection rule $\triangle M = \pm 1$, $\triangle m = 0$ no longer holds in our case since the directions of nuclear quantization before and after the electronic transition are no longer the same. This is illustrated in figure 2. Although the nuclear spin states $|m_j(M)\rangle$ and $|m_j(M-1)\rangle$ before and after the transition have different directions of quantization from each other, they can be expressed in a common coordinate system. The required transformation coefficients are given for example, by Rose (1957). The eigenfunctions for $I=3/2$ are:

$$\left|\tfrac{3}{2}(M)\right\rangle = \cos^3\frac{\theta M}{2}\left|\tfrac{3}{2}\right\rangle + \sqrt{3}\cos^2\frac{\theta M}{2}\sin\frac{\theta M}{2}\left|\tfrac{1}{2}\right\rangle$$

$$+\sqrt{3}\cos\frac{\theta M}{2}\sin^2\frac{\theta M}{2}\left|-\tfrac{1}{2}\right\rangle + \sin^3\frac{\theta M}{2}\left|-\tfrac{3}{2}\right\rangle.$$

$$\left|\tfrac{1}{2}(M)\right\rangle = -\sqrt{3}\cos^2\frac{\theta M}{2}\sin\frac{\theta M}{2}\left|\tfrac{3}{2}\right\rangle$$

$$+\left(\cos^3\frac{\theta M}{2}-2\cos\frac{\theta M}{2}\sin^2\frac{\theta M}{2}\right)\left|\tfrac{1}{2}\right\rangle$$

$$+\left(2\cos^2\frac{\theta M}{2}\sin\frac{\theta M}{2}-\sin^3\frac{\theta M}{2}\right)\left|-\tfrac{1}{2}\right\rangle$$

$$+\sqrt{3}\cos\frac{\theta M}{2}\sin^2\frac{\theta M}{2}\left|-\tfrac{3}{2}\right\rangle.$$

$$\left|-\tfrac{1}{2}(M)\right\rangle = \sqrt{3}\cos\frac{\theta M}{2}\left|\tfrac{3}{2}\right\rangle$$

$$+\left(-2\cos^2\frac{\theta M}{2}\sin\frac{\theta M}{2}+\sin^3\frac{\theta M}{2}\right)\left|\tfrac{1}{2}\right\rangle$$

$$+\left(\cos^3\frac{\theta M}{2}-2\cos\frac{\theta M}{2}\sin^2\frac{\theta M}{2}\right)\left|-\tfrac{1}{2}\right\rangle$$

$$+\sqrt{3}\cos^2\frac{\theta M}{2}\sin\frac{\theta M}{2}\left|-\tfrac{3}{2}\right\rangle$$

$$\left|-\frac{3}{2}(M)\right\rangle = -\sin^3\frac{\theta M}{2}\left|\frac{3}{2}\right\rangle + \sqrt{3}\cos\frac{\theta M}{2}\sin^2\frac{\theta M}{2}\left|\frac{1}{2}\right\rangle$$

$$-\sqrt{3}\cos^2\frac{\theta M}{2}\sin\frac{\theta M}{2}\left|-\frac{1}{2}\right\rangle + \cos^3\frac{\theta M}{2}\left|-\frac{3}{2}\right\rangle$$

where, θM is the polar angle for the vector $\xi_j(M)$ along which the nuclear spin is quantized.

From eq. (A.6),

$$\xi_j(M) = \eta_j(M)\cdot \mathbf{p}/|\eta_j(M)|.$$

Substituting for $\eta_j(M)$ from eq. (A.5), and for $|\eta_j(M)|$ from eq. (A.7), we have,

$$\xi_j(M) = \begin{pmatrix} \left(1{\cdot}29 + \dfrac{24{\cdot}7M}{|g|}\right)\sin\theta \\ 0 \\ \left(1{\cdot}29 + \dfrac{127{\cdot}8M}{|g|}\right)\cos\theta \end{pmatrix} \Bigg/ \left[\sin^2\theta\left(1{\cdot}29+\frac{24{\cdot}7M}{|g|}\right)^2 + \cos^2\theta\left(1{\cdot}29+\frac{127{\cdot}8M}{|g|}\right)^2\right]^{1/2} \tag{A.10}$$

By substituting for M the values -1, 0 or $+1$, the $\xi_j(M)$ vectors can be found out. The $\xi_j(0)$ vector is found to be along the magnetic field vector $\mathbf{p}$. Thus $\theta_0 = 0°$. The angle between any two of the above three vectors is given by the dot product between the respective vectors. Thus, when the magnetic field is along the direction of maximum zero field splitting D_z, we have $\theta = 25°$ and $\theta_{-1} = 110°$, $\theta_{+1} = 24°$, where, θ_{-1} is the angle between $\xi_j(0)$ vector and $\xi_j(-1)$ vector and θ_{+1} is the angle between $\xi_j(0)$ vector and $\xi_j(+1)$ vector. For $H \parallel D_{\max}$, $\theta = 47°$ and $\theta_{+1} = 30°$, $\theta_{-1} = 130°$.

We thus find that the $\xi_j(-1)$ vector changes by more than 90° for the electronic transition $|0\rangle \longleftrightarrow |-1\rangle$. The $\xi_j(+1)$ vector changes by less than 90° for the $|0\rangle \longleftrightarrow |+1\rangle$ transition. The transition probability is given by the equation

$$I[M, M-1; m_1(M)\, m_2(M); m'_1(M-1)\, m'_2(M-1)] \propto \langle m_1(M)\,|\,m'_1(M-1)\rangle^2 \langle m_2(M)\,|\,m'_2(M-1)\rangle^2 \tag{A.11}$$

The total number of possible combination of $(m_1(M)m_2(M); m'_1(M-1)\, m'_2(M-1))$ for a case where $I = 3/2$ is 256 and are given in table 1. The positions of the hyperfine lines with respect to the centre of each fine structure transition and the intensities of the hyperfine lines for $H \parallel D_{\max}$ are also given in table 1.

References

Al'tshuler S A, Kirmse R and Solovev B V 1975 *J. Phys.* **C8** 1907
Cowsik R K, Rangarajan G and Srinivasan R 1971 *Chem. Phys. Lett.* **8** 136
Cowsik R K and Srinivasan R 1973 *Pramāna* **1** 177
Minakata K and Iwasaki M 1972 *Mol. Phys.* **23** 1115
Rose M E 1957 *Elementary theory of angular momentum* (New York: John Wiley and Sons and London: Chapman & Hall Ltd.) page 52
Slichter C P 1955 *Phys. Rev.* **99** 479
Van Rens J G M, Van Der Drift E and De Boer E 1972 *Chem. Phys. Lett.* **14** 113